Design of catalytic metal-organic assemblies via shape complementarity and conformational constraints in dual curvature ligands

Cui-Lian Liu,[a] Eduard O. Bobylev,[b] Brice Kauffmann,[c] Koen Robeyns,[a] Yann Garcia,[a] Joost N. H. Reek[b] and Michael L. Singleton*[a]

[a] Dr. C. -L. Liu, Dr. K. Robeyns, Prof. Dr. Y. Garcia, Prof. Dr. M. L. Singleton
Institute of Condensed Matter and Nanosciences
Université catholique de Louvain
Place Louis Pasteur 1, Louvain-la-Neuve, 1348, Belgium
E-mail: m.singleton@uclouvain.be

[b] E. O. Bobylev, Prof. Dr. J. N. H. Reek
Van 't Hoff Institute for Molecular Sciences
University of Amsterdam
Science Park 904, Amsterdam 1098 XH, The Netherlands

[c] Dr. B. Kauffmann
Université de Bordeaux CNRS, INSERM, UMS3033
Institut Européen de Chimie et Biologie (IECB)
2 rue Robert Escarpit, 33600 Pessac, France

Supporting information for this article is given via a link at the end of the document.((Please delete this text if not appropriate))

Abstract: Three aromatic amide based ligands (**L1**-**L3**) with a central 1,8-diazatriptycene core were designed and used for self-assembly with Pd^{2+}. While hundreds of stereoisomers based on the conformational flexibility around the amides and the unsymmetrical non-planar structure of the core are possible upon coordination with the metal, the constraints designed into the ligands direct the self-assembly towards only a single Pd_2L_4 cage (**L1**) or Pd_4L_8 double-walled metallomacrocycle (**L2**) structure, even in mixtures of the ligands. We further demonstrate that this structural strategy and the modularity of the ligand synthesis affords ready access to deep endohedral functionalized Pd_4L_8 cavitands (**L3**) capable of catalyzing the tandem hydrolysis of benzaldehyde dimethyl acetal followed by condensation with anthranilamide to give 2,3-dihydroquinazolinones with >1000 fold initial rate enhancements.

Introduction

Self-assembly and folding play essential roles in the complexity and function of proteins. For example, these processes in enzymes lead to the formation of active site cavities lined with functional groups that promote the range of reactions necessary for life.[1] Over the past decades, the possibility of generating synthetic molecules with similar complexity and functions has inspired significant progress in the design of self-assembled cavitands.[2] While numerous strategies for the self-assembly of such structures have been developed, the combination of organic ligands and metal ions for the formation of metal-organic architectures has risen as a highly promising approach.[3] Notably, the combination of Pd^{2+} or Pt^{2+} with ditopic ligands for the formation of M_nL_{2n} structures has attracted substantial attention and led to some of the largest well-defined systems.[4] A wide range of applications related to their cavities has been reported, including sensing, catalysis, drug delivery, storage, and molecular recognition.[5]

Unlike synthetic building blocks, folding of peptides leads to subunits for self-assembly that have not only complex electrostatic potential surfaces but also a wide diversity of shapes.[6] The resulting high complementarity between different subcomponents allows for the selective self-assembly of different units into complex asymmetric architectures. By contrast, the majority of synthetic strategies for coordination-driven self-assembly rely on rigid ligands with high, often planar, symmetry.[7] This can be readily seen in M_nL_{2n} assemblies. The ligands are most commonly curved organic molecules where N-heterocyclic donor groups are connected by flat aromatic or alkyne spacers, the rigidity of which allows the angle between coordination sites, the bend angle, to be well-defined.[4b, 8] This offers numerous advantages, such as allowing good prediction of the final self-assembled structures and clean formation of single species. Still, the use of lower symmetry ligands could allow additional shape complementarity between ligands to help direct self-assembly, ultimately leading to new design strategies and more complex structures.[9] In the last decade, a number of elegant approaches relying on enhanced shape complementarity for controlling self-assembly have been described, such as combining two different ditopic ligands with compatible convergent and divergent bend angles or the use of coordination sphere engineering.[10] The latter uses additional functional groups included near the coordination sites on the ligands to provide complementarity interligand steric or electrostatic interactions.[11]

Recently, we succeeded in using heteroaromatic amide-based ligands for the self-assembly of multiple Pd_nL_{2n} (n=2, 6, or 12) metal-organic cages capable of neutral guest discrimination.[12] Despite the flexibility around the amide bonds, non-covalent interactions in the ligands lead to preferential curved conformational states that orient the coordination sites and allow sufficient control over the bend angles of the ligands to direct self-assembly. Nevertheless, these ligands are predominately flat and offer only limited interactions between ligands for the self-assembly of metal-organic cages. In fact, this is seen in the

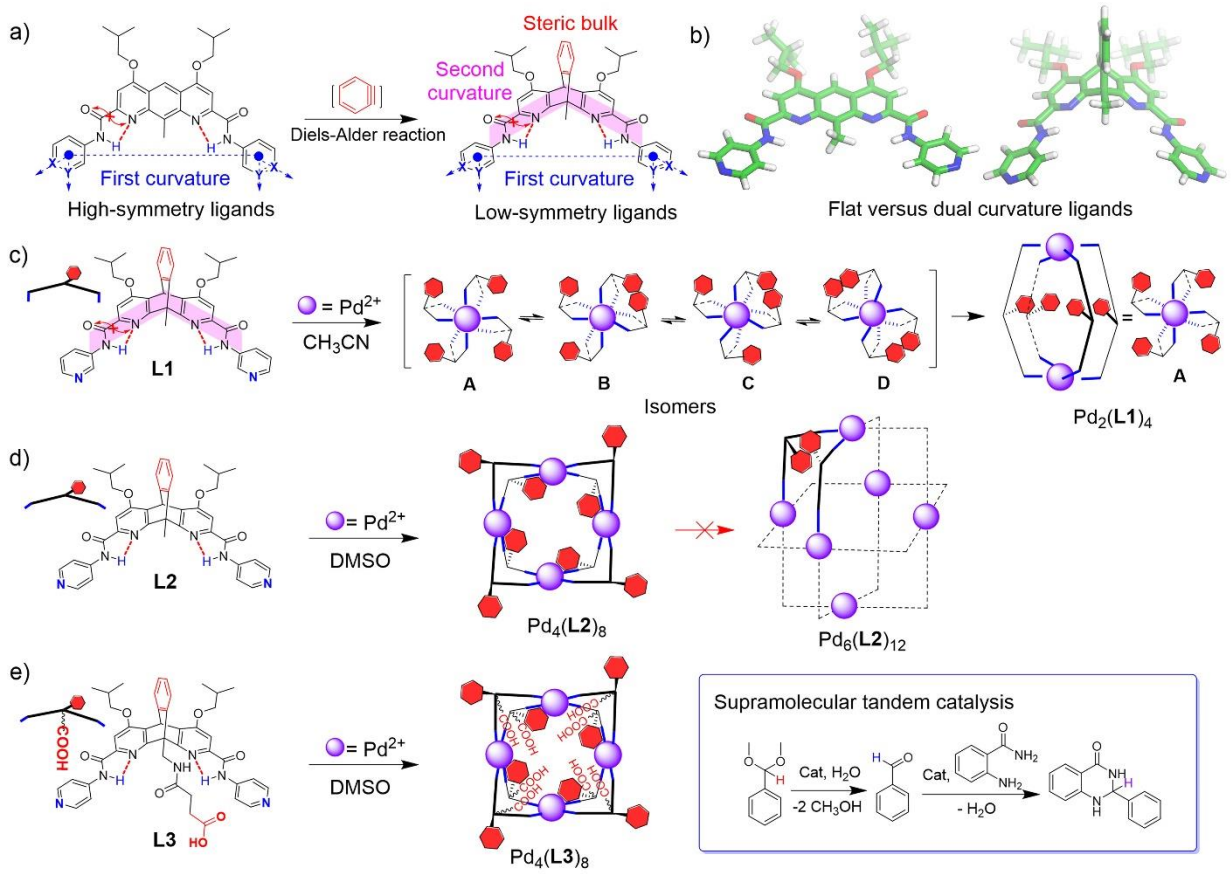

Figure 1 a) Design of aromatic amide-based dual curvature ligands for coordination-driven self-assembly via Diels-Alder reaction with diazaanthracenes. This breaks the ligand symmetry and introduces additional shape complementarity as seen in the density functional theory (DFT) calculated structures of b) flat versus dual curvature ligands. c-e) the structure of ligands **L1-L3** and their self-assembled products that can act as catalysts for the tandem reaction sequence shown in the inset.

majority of ligands used for the self-assembly of M_nL_{2n} assemblies.[4] Modification of the surface of the flat aromatic units to include perpendicular interactions is a challenge. However, this can be the fastest way to direct groups towards other ligands for designing interligand interactions and shape complementarity. We have recently shown that the large diazaanthracene units used for our ligands are amenable to modification via Diels-Alder reaction leading to diazaiptycene or triptycene units.[13] These motifs are intriguing for incorporating additional shape complementarity aspects, remote from the coordination sites, into heteroaromatic amide ligands for self-assembly. In effect, the reaction of the central ring in the diazaanthracene bends the attached N-heterocyclic rings towards each other, a change which, in the ligand structure, adds an additional curvature perpendicular to the curvature that defines the bend angle, Figure 1a. Herein, we demonstrate that this dual curvature, combined with the electrostatic interactions that dictate the bend angle, can direct self-assembly towards a single M_2L_4 cage or M_4L_8 double-walled metallomacrocycle out of the hundreds of possible stereoisomers that could result from different combinations of amide conformation and triptycene unit orientation, Figures 1 and S10. Using this strategy, we further show that the high modularity of the amide ligands allows ready access to deep endohedral functionalized cavitands capable of tandem catalysis.

Results and Discussion

Ligand design and synthesis - Diazatriptycene ligands **L1** and **L2** were synthesized in three steps from the reported 1,8-diazaanthracene-2,7-dicarboxylate ester,[13b] Scheme 1, starting with a [4+2] cycloaddition between in situ generated benzyne. Subsequent saponification and amide coupling with either 3-aminopyridine or 4-aminopyridine gave ligands **L1** and **L2** in 68 and 87% yield, respectively. The Diels-Alder reaction with benzyne bends the ligands introducing the second curvature of ~120° between the planes of the amide groups based on the calculated structures, Figure 1a. Additionally, it adds a large benzene ring on one face of the ligand, which is expected to act as a source of steric hinderance between ligands to help control the self-assembly.

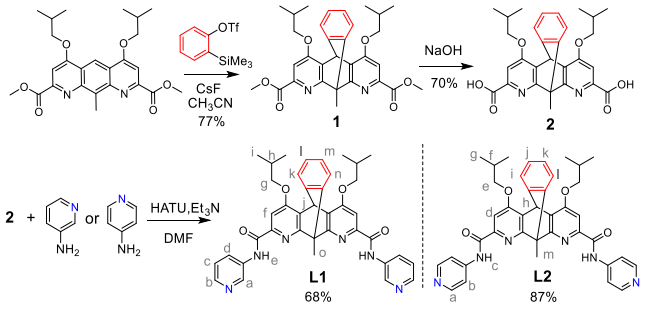

Scheme 1. Synthetic procedures for ligands **L1** and **L2.**

Self-Assembly with L1 and L2 - Complexation of **L1** with Pd^{2+} (NO_3^-, BF_4^-, $CF_3SO_3^-$, or PF_6^- salt) in a 2:1 molar ratio in CD_3CN or D_7-DMF at 40 ℃ results in a clear yellow solution. After two hours, the ^1H NMR spectrum shows a single sharp set of signals with the same number of resonances as the starting ligand, Figure 2a-b and Figure S4-S7. Compared to **L1**, significant shifts of several resonances are observed. Notably, protons H_a and H_b of the pyridine groups appear further downfield, implying coordination of pyridine to Pd^{2+}. These observations suggest the formation of a single symmetric species derived from the complexation of **L1** with Pd^{2+} ions. Based on the expected parallel coordination vectors of the ligand, this was proposed to be an M_2L_4 structure. Consistent with this, diffusion-ordered ^1H NMR (DOSY) showed that all the proton resonances had the same diffusion coefficient of D =6.99×10^{-10} m^2/s, which, based on the Stokes-Einstein equation, indicates a small structure with a radius of 8.3 Å, Figure 2c. Electrospray ionization time-of-flight mass spectrometry (ESI-TOF-MS) further supported this assignment; a series of isotopic patterns corresponding to $[Pd_2(\mathbf{L1})_4(BF_4)_{4-n}]^{n+}$ (n=2-4) were observed, Figure 2d.

For this species, the symmetry and single set of signals observed by NMR are interesting because the different *syn/anti* orientations around the amides or *cis/trans* orientations of the ligand backbones could lead to hundreds of possible stereoisomers, Figure 3 and Figure S8-S10. These nevertheless appear to converge to a single stable species, and time-dependent NMR studies of the self-assembly of **L1** did not show any clear signs of other isomers forming as intermediates, Figure S5. Within ten minutes of mixing the ligand with Pd^{2+} ions, the ^1H NMR of the solution exhibited relatively broad signals with low intensity. ESI-TOF-MS analysis of the solution mainly found $Pd_2(\mathbf{L1})_4(BF_4)_4$ suggesting the composition of this mixture was predominately the M_2L_4 cage with possibly some oligomers and intermediates from the self-assembly. After one hour, only a single sharp set of resonances, as observed above, emerges and becomes the significant species by ^1H NMR. In the presence of dimethyl sulfone as an internal standard, the observed signals account for >90% of the ligand used for self-assembly, Figure S7.

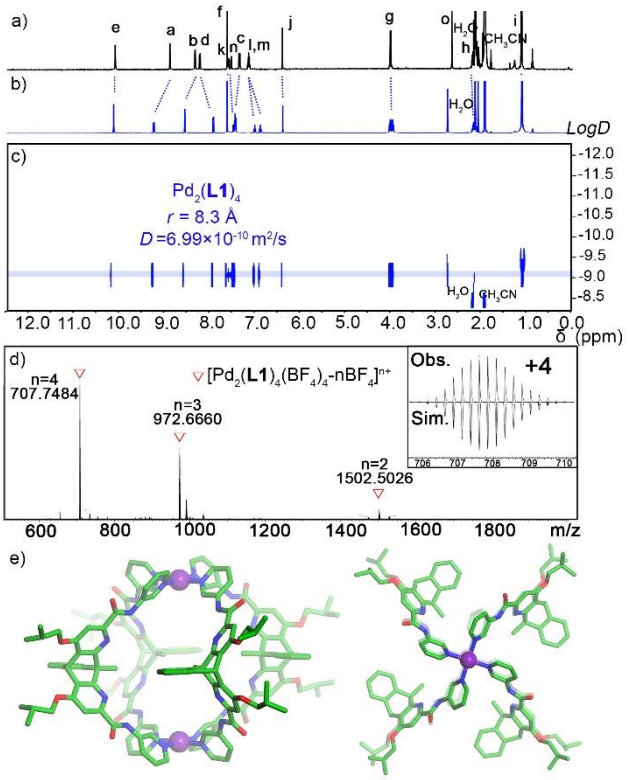

Figure 2. ^1H NMR spectra (500 MHz, CD_3CN, 298 K) of ^1H NMR spectra of a) **L1** and b) its self-assembly product $Pd_2(\mathbf{L1})_4$. c) the DOSY spectra of $Pd_2(\mathbf{L1})_4$. d) ESI-TOF-MS for $Pd_2(\mathbf{L1})_4$ as its BF_4^- salt. Inset shows the comparison of the observed isotopic pattern with the simulated spectrum. e) X-ray crystal structure of $Pd_2(\mathbf{L1})_4$ with views perpendicular to (left) and along (right) the Pd-Pd axis. Protons, solvent molecules and counterions are omitted for clarity.

Relative to the possibility of different conformations, density functional theory (DFT) computational studies (B3LYP/6-31g*) support that the *anti*-conformation(**L1A**) between the amides of ligand **L1** (possible ligand isomers, **L1A**, **L1B**, and **L1C**) should be favored by almost 30 kJ/mol in the self-assembly solvent (CH_3CN), Figure 3a. Similar studies (B3LYP/def2SVP) on the M_2L_4 cage also suggest that this preference should be maintained in the complex, Figure 3b. Still, the lack of planar symmetry in the ligands could result in four different $Pd_2(\mathbf{L1})_4$ isomers (A-D) with different *cis/trans* relationships between the 9,10-bridging groups, Figure 3c. However, the dual curvature designed into the ligands should allow for good shape complementarity that directs single isomer formation in order to avoid steric interactions between neighboring ligands. Indeed, additional DFT studies comparing the four isomers estimated that isomer A, where the curves of the ligands are oriented in the same direction, should be the most stable by ~40 kJ/mol. Based on the calculated structures, the higher energy for the three other isomers likely results from steric interactions between nearby benzene rings in the diazatriptycene backbones.

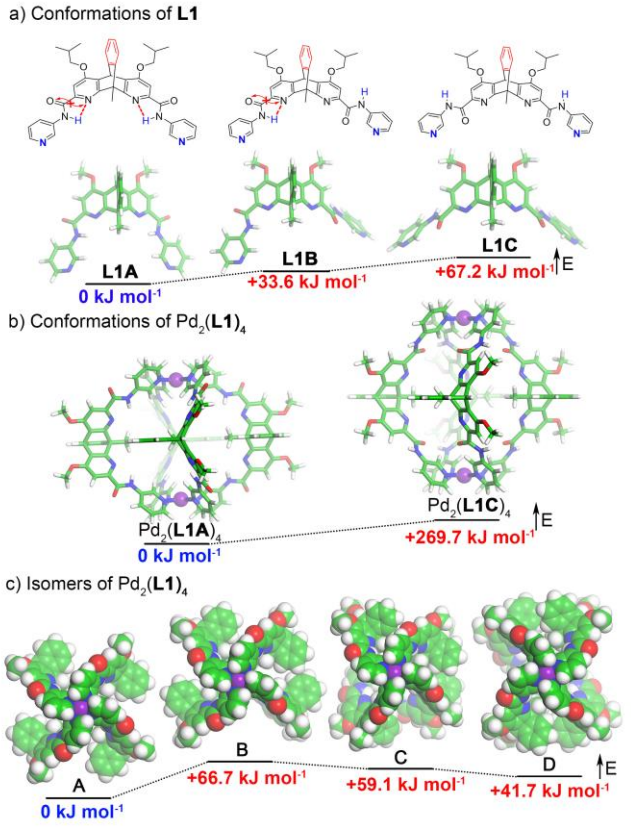

Figure 3. Density functional theory (DFT) calculated structures and relative energies(B3LYP/6-31g* for ligands and B3LYP/def2SVP for cages) of a) three possible conformations of ligand **L1**(**L1A**, **L1B** and **L1C**), b) Pd_2(**L1**)$_4$ cage with representative ligand *syn*/*anti* amide conformations, and c) four possible diastereomers of Pd_2(**L1**)$_4$ cage based on triptycene orientation.

Further support for the formation of isomer A came from its solid-state structure. Single crystals of Pd_2(**L1**)$_4$(BF_4)$_4$ could be obtained and were studied by X-ray diffraction, Figure 2e. The crystal structure of the complex shows two palladium ions, each in a square planar N_4 coordination environment, bridged by four units of **L1** with a Pd^{2+} to Pd^{2+} distance in the cage of 12.3 Å. In accordance with the solution observations and computational results, the benzene rings on the ligands are all oriented in the same direction around the four-fold symmetry axis, and the amide carbonyls are all *anti* to the endocyclic nitrogens of the diazatriptycene units. Relative to our previously reported M_2L_4 cage,[12] which had overall D_{4h} symmetry, the directionality of the triptycene units used for Pd_2(**L1**)$_4$ leads to a decrease in the symmetry of the cage to C_{4h}.

Motivated by the high selectivity observed with ligand **L1**, we next looked to see if the self-assembly of larger structures using the reduced symmetry ligands could still be controlled by the dual curvature effects. Ligand **L2** was reacted with 0.5 equivalents of Pd^{2+} (NO_3^-, BF_4^-, $CF_3SO_3^-$, or PF_6^- salt) in D_6-DMSO or D_7-DMF. Similar to self-assembly with **L1**, the ^{1}H NMR spectrum showed a single set of resonances distinct from the starting ligand, Figure 4a-b and Figure S11-S14. Again, using an internal standard indicates that >90% of [**L2**] is represented by this new species, Figure S14. As expected, DOSY studies on this species suggested the formation of a larger structure (D = 7.32×10^{-11} m^2/s; r= 13.8 Å), Figure 4c. However, as opposed to the M_6L_{12} or $M_{12}L_{24}$ cages obtained previously with the analogous planar ligand,[12] ESI-TOF-MS analysis showed isotopic patterns consistent with the formation of an M_4L_8 assembly with the formula Pd_4(**L2**)$_8$(BF_4)$_8$, Figure 4d. This composition was further confirmed by X-ray diffraction studies. The crystal structure shows a deep crown-like double-walled metallomacrocycle, Figure 4e. The four palladium ions are found in the same plane and can be seen as occupying the four corners of a square. Each palladium has square-planar coordination, with two ligands, one above and one below the plane, bridging between each pair of adjacent metal ions. This gives a structure with cavity dimensions of 20.5 Å between opposite palladiums and 23.8 Å between the top and bottom faces. All of the ligands are oriented in the same way, with the benzene ring of the diazatriptycene units in each bridging pair pointing away from each other towards either the top or bottom of the structure. This also results in the 9-position group on the diazatriptycene units of the ligands converging towards the center of the cavity.

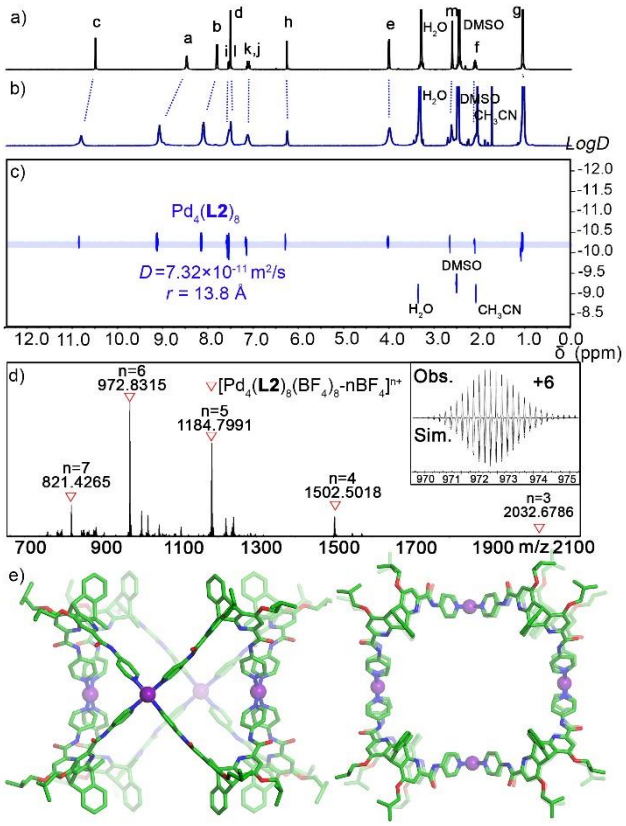

Figure 4. ^{1}H NMR spectra (500 MHz, DMSO-d_6, 298 K) of a) **L2** and b) its self-assembly product Pd_4(**L2**)$_8$, and c) the DOSY spectra of Pd_4(**L2**)$_8$. d) ESI-TOF-MS for Pd_4(**L2**)$_8$ as its BF_4^- salt. Inset shows the comparison of the observed isotopic pattern with the simulated spectrum. e) X-ray crystal structure of Pd_4(**L2**)$_8$ with side (left) and top (right) views. Protons, solvent molecules and counterions are omitted for clarity.

Interestingly, the bend angle for the ligands in the crystal structure of Pd_4(**L2**)$_8$ is ~70°, while the same bend angle in the DFT optimized structure of the free ligands was found to be ~60°. Previously, we observed that the partial flexibility in the amide bonds could allow changes of almost 30° in the bend angle,

making it possible to transition from a smaller cage structure to a larger one.[12] For example, M_6L_{12} and $M_{12}L_{24}$ structures, which require ideal bend angles around 90° and 120°, respectively, could be formed with the same aromatic amide ligand in a step-wise manner. With this in mind, we attempted to push the self-assembly of Pd_4(**L2**)$_8$ towards a larger Pd_6(**L2**)$_{12}$ octahedron. However, even after extending the time for self-assembly up to two weeks or increasing the temperature to 120 ℃, no other apparent species were observed by NMR nor ESI-TOF-MS analysis. The cube-like structures in most M_6L_{12} octahedra contain eight adjacent 3-fold symmetry axes. With the dual curvature ligand **L2**, it is impossible for the ligands to be arranged in a way where they are all pointing away from each other, something that can occur with Pd_4(**L2**)$_8$, Figure 4e. Interestingly, no close contacts of the complementary shapes, as seen in the isomers of Pd_2(**L1**)$_4$, are observed in a PM6 model of a Pd_6(**L2**)$_{12}$ octahedron, Figure S15. Thus, it is suspected that a combination of unfavorable ligand orientation and significant distortions in the torsion angles around the amides may limit the stability of the M_6L_{12} structure.

Self-Sorting Studies - To look at how strongly the non-covalent interactions present in the ligand structures control their bend angle, self-sorting studies were performed. In theory, changes in the torsion angles around the amides, at the expense of weakening the non-covalent interactions, should permit both ligands to achieve the same bend angles. While this could potentially allow the self-assembly of structures containing both ligands **L1** and **L2**, this does not appear to be favored. Indeed, upon reacting a 1:1 mixture of **L1** and **L2** with $Pd(CH_3CN)_4(BF_4)_2$ in D_7-DMF, two distinct sets of signals corresponding to the M_2(**L1**)$_4$ and M_4(**L2**)$_8$ species as described above were observed by ^{1}H NMR, Figure 5 and Figure S20. ESI-TOF-MS analysis also showed only a mixture of M_2L_4 and M_4L_8 species. These observations indicate that, despite the weak nature of the non-covalent interactions that direct the ligand conformation, they still provide sufficient control to allow self-sorting based on bend angle, something only previously reported for more ridged ligands.[14]

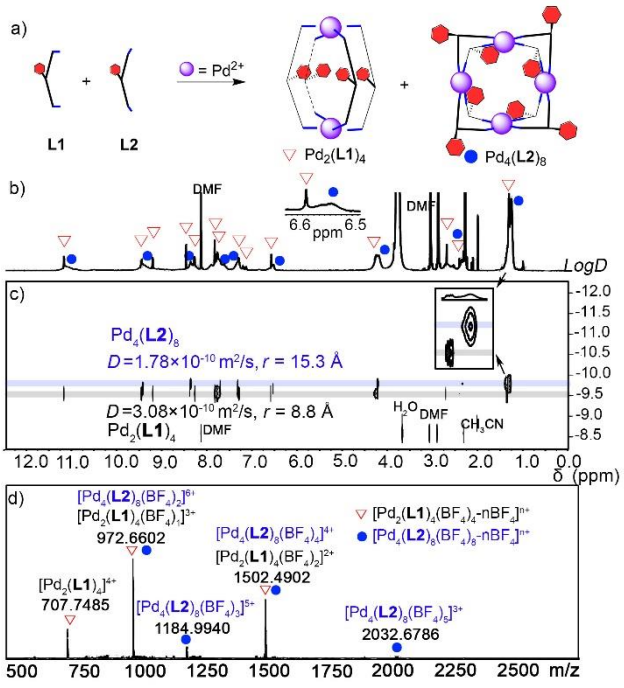

Figure 5. a) Narcissistic self-sorting of M_2L_4 and M_4L_8 architectures from mixed ligands. b) ^{1}H NMR spectra (500 MHz, DMF-d_7, 298 K), c) the DOSY spectra and d) ESI-TOF-MS of self-sorting outcomes showing a mixture of M_2(L1)$_4$ and M_4(L2)$_8$ species.

Cage functionalization – Metal-organic architectures offering defined microenvironments for specific host-guest interactions are of interest for developing enzyme active site mimics. The confined spaces in these structures have been reported to give significant rate enhancements and product selectivity for a range of organic reactions.[5f, 15] While the smaller cavity in Pd_2(**L1**)$_4$ limits the potential for having both endohedral functionalization and guest binding, the larger M_4L_8 structure is an intriguing scaffold for designing functional group lined cavities for catalysis. From the structure, the large openings in the top and bottom faces of the host can easily allow substrate and product diffusion in or out of the deep cavity. Moreover, the defined orientation of the diazaanthracene 9-position and modularity of the ligand design can facilitate the endohedral functionalization of the structure. To this end, ligand **L3** bearing a carboxylic acid function was synthesized as shown in Scheme 2. Following reported procedures, the 9-methyl in the precursor 1,8-diazaanthracene-2,7-dicarboxylate ester could be easily functionalized into a Boc-protected 9-methylamino diazaanthracene derivative.[16] Next, triptycene formation and installation of the pyridine coordination sites were performed in a manner analogous to **L2**. Subsequent amine deprotection and reaction with succinic anhydride allowed the incorporation of the carboxylic acid group in **L3**.

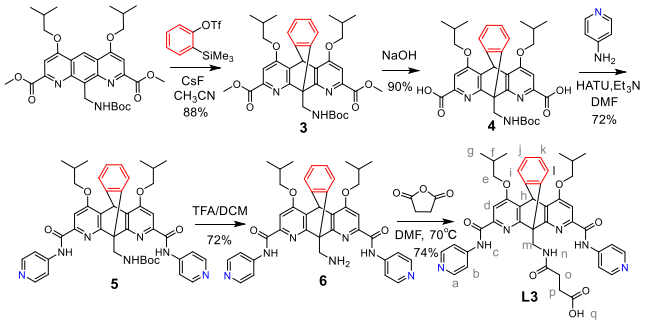

Scheme 2. Synthetic procedures for ligands **L3.**

Despite potential for the endohedral carboxylic acid to compete with metal-pyridine interactions,[3c, 17] self-assembly with **L3** proceeded without any problems. Upon reaction of **L3** with Pd^{2+} (NO_3^-, BF_4^-, $CF_3SO_3^-$, or PF_6^- salt), in a 2:1 molar ratio in D_6-DMSO or D_7-DMF, similar changes as for self-assembly with **L2**, i.e., a single set of signals shifted relative to the free ligand, are seen by ^{1}H NMR, Figure 6a-b and Figure S16-S19. Given the similar bend angles expected for **L2** and **L3**, self-assembly with the functionalized ligand should also lead to an M_4L_8 structure. This was supported by DOSY studies (D = 7.55×10^{-11} m^2/s; r = 13.4 Å), which suggested the formation of a complex with a size similar to parent Pd_4(**L2**)$_8$, Figure 6c. The Pd_4(**L2**)$_8$(BF_4)$_8$ formula was further confirmed by ESI-TOF-MS, though some low-intensity signals for an M_5L_{10} structure could also be observed, Figure 6d. The presence of the more bulky group on the 9-position of **L3** relative to **L2** may lead to this minor formation of some of the larger macrocycles.[14a, 18] Still, the species observed by NMR represents >90% of ligand used for self-assembly. Additionally, the X-ray crystal structure of the product showed Pd_4(**L3**)$_8$ and was highly similar to the M_4(**L2**)$_8$ structure, Figure 6e. The 9-position substituents are still found pointing into the cavity and oriented towards each other such that they occupy the cavity windows formed by the pairs of bridging ligands. This also leads to short distances between neighboring carboxylic acid groups (O-O distances of 2.3 -2.7 Å), suggesting potential hydrogen bond formation between these groups. Such interactions might be expected to lead to some preference for self-sorting. However, self-assembly with mixtures of **L3** and **L2** resulted in statistical mixtures of M_4L_8 species with different ratios of the two ligands, though similar studies using **L3** and **L1** still showed self-sorting into M_2(**L1**)$_4$ and M_4(**L3**)$_8$ based on the different bend angles, Figure 7 and Figure S21-S24.

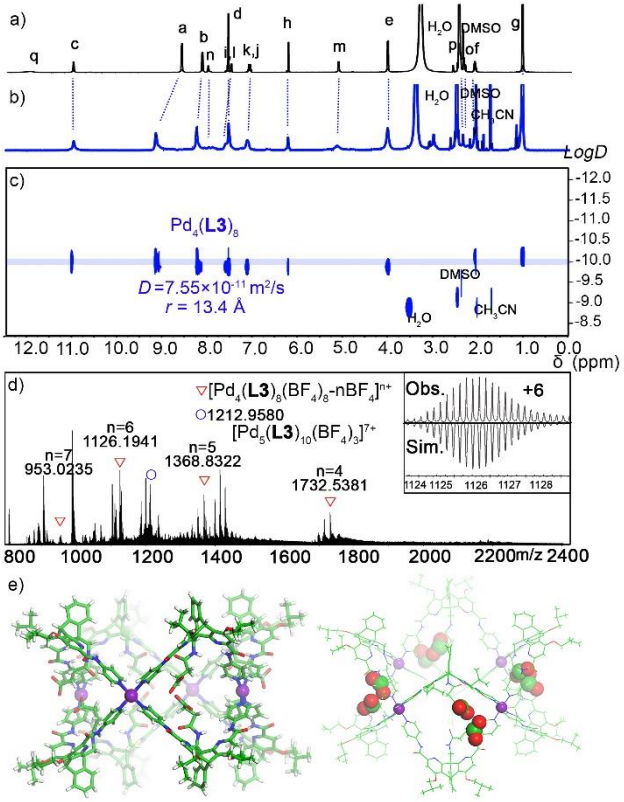

Figure 6. ^{1}H NMR spectra (500 MHz, DMSO-d_6, 298 K) of ^{1}H NMR spectra of a) **L3** and b) its self-assembly product Pd_4(**L3**)$_8$. c) the DOSY spectra of Pd_4(**L3**)$_8$. d) ESI-TOF-MS for Pd_4(**L3**)$_8$ as its BF_4^- salt. Inset shows the comparison of the observed isotopic pattern with the simulated spectrum. e) X-ray crystal structure of Pd_4(**L3**)$_8$ with side views (left) and highlighting the 9-position endohedral carboxylic acids (right). Solvent molecules and counterions are omitted for clarity.

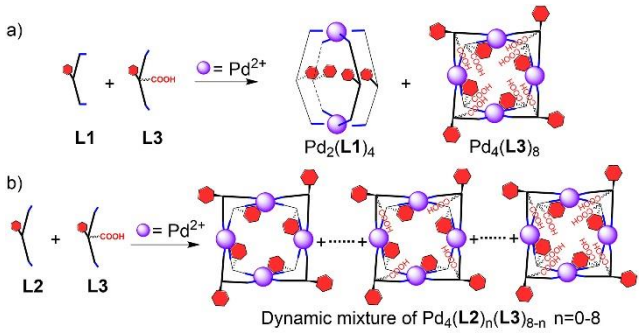

Figure 7. Mixed ligands self-assembly with ligand **L3,** mixed with a) **L1** leads to narcissistic self-sorting of M_2(**L1**)$_4$ and M_4(**L3**)$_8$ assemblies and b) **L2** formed non-sorted scrambled dynamic mixtures of Pd_4(**L2**)$_n$(**L3**)$_{8-n}$(BF_4)$_8$, n=0-8.

Catalysis - Based on the carboxylic acid functions in ligand **L3**, we were interested in studying the reactivity of the endohedral functionalized M_4L_8 structures. For this, we chose to look at a tandem reaction sequence involving hydrolysis of benzaldehyde dimethyl acetal followed by aminal formation with anthranilamide to give 2,3-dihydroquinazolinones. This class of molecules is a useful privileged scaffold in medicinal chemistry due to their range of pharmacological activities.[19] Importantly, both reaction steps can be catalyzed by either Lewis or Bronsted

acids. Heterogeneous catalysis of the overall sequence has been previously demonstrated with acid functionalized metal-organic frameworks and the second step has been shown to be catalysed by a Zn based metal-organic cage at higher temperatures.[20] However, the room temperature catalysis of the tandem sequence has not been described with discrete metal-organic cages, making the endohedral acid functionalized Pd_4(**L3**)$_8$ highly interesting for this transformation.

The reactivity of the assemblies, Pd_4(**L3**)$_8$, Pd_4(**L2**)$_8$ or Pd_2(**L1**)$_4$, as catalysts for the tandem 2,3-dihydroquinazolinones synthesis (reaction 3, Table 1), as well as the individual acetal hydrolysis (reaction 1, Table 1) and aminal formation steps (reaction 2, Table 1), was studied and compared to the control complexes, $Pd(DMAP)_4$ and $Pd(acetate)_2$, and the free ligands **L3**, **L2**, and **L1**. In all cases, the reactions were performed with substrates at concentrations of ~40mM. Catalyst concentrations were chosen to keep Pd^{2+} or ligand concentration constant, i.e. 3.1 mol% Pd_4(**L3**)$_8$ or Pd_4(**L2**)$_8$, 6.2 mol% Pd_2(**L1**)$_4$, 24.8 mol% $Pd(DMAP)_4$ or $Pd(acetate)_2$, or 24.8 mol% **L3**, **L2** or **L1**. Product formation was followed by ^{1}H NMR using dimethyl sulfone as an internal standard. Based on a screening of the reaction with Pd_4(**L3**)$_8$ in different solvents, Table S2, the best yields were obtained with wet acetonitrile. The initial rates and TOF for the first three hours of the reactions, as well as the yields for the reactions in CD_3CN, are summarized in Table 1 and Figures S26-S55.

Substantial rate enhancements are observed for all of the reactions with the self-assembled structures. Initially, we studied the acetal hydrolysis to benzaldehyde (Reaction 1: **A** to **B**) in wet acetonitrile, Table 1 and Figures S26-S35. With Pd_4(**L3**)$_8$, it occurs rapidly at room temperature. The initial rate calculated for this cage was found to be 1778 $\times10^{-4}$ mM/min (TOF = 8.9 h^{-1}) and the yield of product **B** after 24 h was 92%. This is about 1.9 times faster than for either the parent Pd_4(**L2**)$_8$ or Pd_2(**L1**)$_4$, which lack the endohedral functionalization and the initial TOF is ~8 times higher than a related endohedral functionalized Fe^{2+} cage, reported recently as a catalyst for this step.[21c] Importantly, even for these unfunctionalized cages, control studies suggest that the larger assembled structures are important for their observed catalytic reactivity. With the unfunctionalized ligands **L2** and **L1** or the monomeric Pd^{2+} complexes, no appreciable reaction was observed. Indeed, only ligand **L3** gave moderate product formation, with an initial reaction rate of 44 $\times10^{-4}$ mM/min (TOF = 0.03 h^{-1}). This is due to the presence of the carboxylic acid group as expected. Nevertheless, even keeping the concentration of the carboxylic acid groups equal, the initial rate enhancement with Pd_4(**L3**)$_8$ represents an almost 4000% increase over its free ligand **L3**.

Moving to the second reaction (Reaction 2: **B** + **D** to **C**), the condensation of benzaldehyde with 2-aminobenzamide showed largely similar trends, Table 1 and Figures S36-S45. The initial rate with Pd_4(**L3**)$_8$ was 733$\times10^{-4}$ mM/min (TOF = 3.55), while for Pd_4(**L2**)$_8$ and Pd_2(**L1**)$_4$, it was found to be 533 $\times10^{-4}$ mM/min (TOF = 2.58) and 667 $\times10^{-4}$ mM/min (TOF = 1.64) respectively. The unfunctionalized ligands and the mononuclear complexes gave <2% product formation even after 24 hours. As expected, the carboxylic acid-containing **L3** functions better but still shows a much lower initial rate and TOF, 200 $\times10^{-4}$ mM/min and 0.13 h^{-1} respectively, than any self-assembled structures.

Encouraged by these results, we next looked at the tandem hydrolysis of benzaldehyde dimethyl acetal and condensation with 2-aminobenzamide, reaction 3: **A** + **D** to **C** Table 1 and Figure S46-S55. Again, when Pd_4(**L3**)$_8$ was used as the catalyst with substrates **A** and **D**, the starting acetal disappeared rapidly, coinciding with the formation of **C**. The initial reaction rate for the product formation was calculated to be 489$\times10^{-4}$ mM/min (TOF = 2.37 h^{-1}). This represents a more than 2000% increase in the initial reaction rates versus the cage components (ligand or monomeric Pd^{2+} complexes). Indeed, the free ligand, **L3**, or the monomeric Pd^{2+} complexes reacted much slower, giving little product (<10%) even over 24h. The same reaction with Pd_4(**L2**)$_8$ or Pd_2(**L1**)$_4$ also leads to significant product formation, though with rates moderately slower (222 $\times10^{-4}$ mM/min, TOF = 1.08 h^{-1} and 444 $\times10^{-4}$ mM/min, TOF = 1.08 h^{-1}) than for Pd_4(**L3**)$_8$.

The collection of reactivities during all steps of the reaction sequence allow for some interesting observations based on the different catalyst structures. First, Pd_4(**L3**)$_8$ gives the highest reactivity even when compared to similar cage structures, suggesting an important effect of the endohedral functionalization. This does not appear to be due to problems related to self-assembly (reactive impurities) nor to additional carboxylate coordinated Pd^{2+} ions. Indeed, Pd_4(**L3**)$_8$ obtained by *in situ* self-assembly, from single crystals formed as described for X-ray crystallographic studies, or by precipitation with diethyl ether and redissolution in CD_3CN, gave similarly high reactivity. Further, the limited reactivity observed for $Pd(acetate)_2$, and lack of evidence of any major species with additional Pd^{2+} coordination by NMR or ESI-TOF MS suggests that Lewis acidic Pd^{2+} carboxylate species[3c, 17] are not likely responsible for the observed reactivity. When 24.8 mol% $Pd(MeCN)_4BF_4$ is used alone as catalyst for the tandem reaction sequence, product formation is also observed with a TOF (2.69 h^{-1}) comparable to those of the cages. However, this concentration of free palladium far exceeds what is possible with the cages, and lower concentrations are less reactive than Pd_4(**L3**)$_8$. Additionally, with loadings between 3 - 24.8% of $Pd(MeCN)_4BF_4$ a black precipitate, presumed to be palladium black, forms shortly after addition of the substrates. No such precipitate is observed in the presence of the ligands and, by NMR, the cage remains intact both during and after the reaction. Thus, while we cannot entirely rule out that free Pd^{2+} ions in solution may have a minor contribution to the catalysis, the high reactivity observed when Pd_4(**L3**)$_8$ is used as the catalyst is not the result of free Pd^{2+}.

As a second feature important for the catalysis, given that all of the cages show higher reactivity versus the mononuclear Pd^{2+} complexes or their free ligands, the overall self-assembled structure should be highly important for enhancing the catalysis. Notably, cavity effects in self-assembled cages have been shown to play a major role in facilitating reactions with bound substrates.[18] To look for interaction between the cages and substrates, we compared NMR chemical shifts in the separate cages and substrates and mixtures of the two. In all cases, interaction with the guests is in the fast exchange regime. For Pd_4(**L3**)$_8$, Pd_4(**L2**)$_8$, and Pd_2(**L1**)$_4$, variations in concentration of substrates **A** and **D** lead to noticeable differences in the ^{1}H NMR chemical shifts for the substrates with smaller shifts for some resonances in the cages (max $\Delta\delta$ = 0.005 - 0.01 ppm), Figure S56-S63. Importantly, the most obvious changes are observed for the endohedral groups, specifically, the amide protons and protons on the 9-position substituents. This is most apparent in the smaller cage Pd_2(**L1**)$_4$, where the endohedral CH_3 group shifts by ~ 0.04 ppm, but also seen in the larger Pd_4(**L3**)$_8$, and

Pd_4(**L2**)$_8$ assemblies, suggesting that binding occurs in the cavities or windows of the structures.

Such interactions with the substrates should not only facilitate the reaction with the endohedral carboxylic acid groups in Pd_4(**L3**)$_8$, but this also helps explain the observed reactivity for the unfunctionalized Pd_4(**L2**)$_8$, and Pd_2(**L1**)$_4$. Indeed, as both bound Pd^{2+} ions and hydrogen bonding sites (amides or pyridine C-H groups in the cages) have been shown in the literature to be able to act as Lewis acids to catalyze similar reactions,[21] binding of the guests by the cages could allow better contact with these reactive sites in the assemblies versus only monomeric structures.

Conclusion

In summary, we have provided an effective strategy for controlling palladium based self-assembly with flexible and non-planar ligands by combining endohedral non-covalent interactions in aromatic amides with additional shape complementarity brought by a dual curvature in the ligand. Three asymmetric diazatryptycene amide based ligands were synthesized and used for self-assembly with Pd^{2+}. Impressively, the constraints designed into the ligands provide high stereoselectivity for the self-assembly process, leading to only a single M_2L_4 cage (**L1**) or M_4L_8 double-walled metallomacrocycle (**L2** or **L3**) out of hundreds of possible isomers. Moreover, we show that despite the flexibility around the amide groups in the ligands, the non-covalent interactions arranged on the ligand backbone provide excellent control over the ligand bend angle, allowing narcissistic self-sorting in mixtures of ligands with different bend angles. This demonstrated level of structural control and the high modularity afforded by the amide connectivity can allow rapid access to libraries of diversely functionalized ligands for applications in sensing and catalysis. To highlight this versatility, we show that this strategy can be used to generate endohedrally functionalized M_4(**L3**)$_8$ structures with deep cavities. These structures were found to catalyze the tandem hydrolysis of benzaldehyde dimethyl acetal and condensation with 2-aminobenzamide to give 2,3-dihydroquinazolinones, with >1000% increase in initial reaction rates versus control acids or mononuclear Pd^{2+} complexes. These results give promising new design strategies for coordination-driven self-assembly where additional shape complimentarity between dually curved ligands can be used for the formation of asymmetric diversely functionalized cavities of interest for catalytic applications.

Table 1. Supramolecular catalysis at room temperature

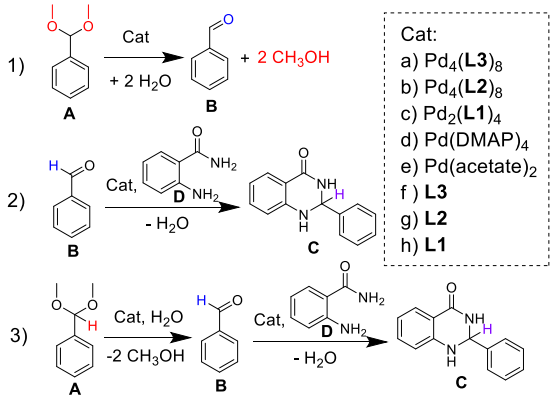

Reactions[a]	Catalyst[b]	Initial rate, × 10^{-4} mM/min	TOF_{init} h^{-1}	Yield[c] %
1) A→B	Pd_4(**L3**)$_8$	1778	8.89	92
	Pd_4(**L2**)$_8$	933	4.51	75
	Pd_2(**L1**)$_4$	955	2.35	69
	$Pd(DMAP)_4$	0.2	n.d.	<2
	$Pd(acetate)_2$	0.5	n.d.	<2
	L3	44	0.03	8
	L2	0.1	n.d.	<2
	L1	n.d.	n.d.	<2
	None	n.d.	n.d.	<2
2) B+D→C	Pd_4(**L3**)$_8$	733	3.55	85
	Pd_4(**L2**)$_8$	533	2.58	69
	Pd_2(**L1**)$_4$	667	1.64	69
	$Pd(DMAP)_4$	0.3	n.d.	<2
	$Pd(acetate)_2$	0.2	n.d.	<2
	L3	200	0.13	35
	L2	n.d.	n.d.	<2
	L1	0.1	n.d.	<2
	None	n.d.	n.d.	<2
3) A+D→C	Pd_4(**L3**)$_8$	489	2.37	90
	Pd_4(**L2**)$_8$	222	1.08	48
	Pd_2(**L1**)$_4$	444	1.08	66
	$Pd(DMAP)_4$	0.2	n.d.	<2
	$Pd(acetate)_2$	0.1	n.d.	<2
	L3	22	0.01	8
	L2	n.d.	n.d.	<2
	L1	0.1	n.d.	<2
	None	n.d.	n.d.	<2

[a] [substrate] = 40mM; [b] 3.1 mol% Pd_4(**L3**)$_8$ or Pd_4(**L2**)$_8$, or 6.2 mol% Pd_2(**L1**)$_4$, or 24.8 mol% Pd(DMAP)$_4$ or Pd(acetate)$_2$ or **L3** or **L2** or **L1** as a catalyst; [c] NMR Yield determined at t = 24h.; n.d. = not able to be determined due to no visible product signals; Initial rates and TOF_{init} were calculated based on the first three hours of reaction.

Acknowledgements

This research was supported in part through the Concerted Research Action (ARC16/21-074) and the China Scholarship Council (pre-doctoral fellowships for C.-L.L.). Computational resources were provided by the supercomputing facilities of the Université catholique de Louvain (CISM/UCL) and the Consortium des équipements de Calcul Intensif en Fédération Wallonie Bruxelles (CPCI) funded by the Fond de la Recherche Scientifique de Belgique (F.R.S.-FNRS) under convention 2.5020.11. We thank Dr S. Ouk for his generous financial support through the Fondation Louvain. We also thank Dr. Gabriella Barozzino for help with NMR measurements.

Keywords: metal-organic cages • isomer selectivity • low-symmetry ligands • supramolecular catalysis

[1] a) C. M. Heckmann, F. Paradisi, *ChemCatChem* **2020**, *12*, 6082-6102; b) R. J. Drout, L. Robison, O. K. Farha, *Coord. Chem. Rev.* **2019**, *381*, 151-160; c) J. Benkovic Stephen, S. Hammes-Schiffer, *Science* **2003**, *301*, 1196-1202.

[2] a) Y. Liu, W. Zhao, C. H. Chen, A. H. Flood, *Science* **2019**, *365*, 159-161; b) Z. Liu, S. K. M. Nalluri, J. F. Stoddart, *Chem. Soc. Rev.* **2017**, *46*, 2459-2478; c) D. S. Kim, J. L. Sessler, *Chem. Soc. Rev.* **2015**, *44*, 532-546; d) G. Gil-Ramírez, D. A. Leigh, A. J. Stephens, *Angew. Chem. Int. Ed.* **2015**, *54*, 6110-6150; e) L. F. Lindoy, K.-M. Park, S. S. Lee, *Chem. Soc. Rev.* **2013**, *42*, 1713-1727; f) T. R. Cook, Y.-R. Zheng, P. J. Stang, *Chem. Rev.* **2013**, *113*, 734-777; g) D. V. Kondratuk, L. M. A. Perdigao, M. C. O'Sullivan, S. Svatek, G. Smith, J. N. O'Shea, P. H. Beton, H. L. Anderson, *Angew. Chem. Int. Ed.* **2012**, *51*, 6696-6699; h) T. Tozawa, J. T. A. Jones, S. I. Swamy, S. Jiang, D. J. Adams, S. Shakespeare, R. Clowes, D. Bradshaw, T. Hasell, S. Y. Chong, C. Tang, S. Thompson, J. Parker, A. Trewin, J. Bacsa, A. M. Z. Slawin, A. Steiner, A. I. Cooper, *Nat. Mater.* **2009**, *8*, 973-978; i) L. R. MacGillivray, J. L. Atwood, *Nature* **1997**, *389*, 469-472.

[3] a) Y.-Q. Zou, D. Zhang, T. K. Ronson, A. Tarzia, Z. Lu, K. E. Jelfs, J. R. Nitschke, *J. Am. Chem. Soc.* **2021**, *143*, 9009-9015; b) E. G. Percástegui, T. K. Ronson, J. R. Nitschke, *Chem. Rev.* **2020**, *120*, 13480-13544; c) A. J. Gosselin, C. A. Rowland, E. D. Bloch, *Chem. Rev.* **2020**, *120*, 8987-9014; d) Y. Sun, C. Chen, P. J. Stang, *Acc. Chem. Res.* **2019**, *52*, 802-817; e) S. Saha, I. Regeni, G. H. Clever, *Coord. Chem. Rev.* **2018**, *374*, 1-14; f) T. R. Cook, P. J. Stang, *Chem. Rev.* **2015**, *115*, 7001-7045.

[4] a) D. Fujita, Y. Ueda, S. Sato, H. Yokoyama, N. Mizuno, T. Kumasaka, M. Fujita, *Chem* **2016**, *1*, 91-101; b) D. Fujita, Y. Ueda, S. Sato, N. Mizuno, T. Kumasaka, M. Fujita, *Nature* **2016**, *540*, 563-566; c) K. Harris, D. Fujita, M. Fujita, *Chem. Commun.* **2013**, *49*, 6703-6712.

[5] a) D. Zhang, T. K. Ronson, Y.-Q. Zou, J. R. Nitschke, *Nat. Rev. Chem.* **2021**, *5*, 168-182; b) S. Yadav, P. Kannan, G. Qiu, *Org. Chem. Front.* **2020**, *7*, 2842-2872; c) M. Zhang, M. L. Saha, M. Wang, Z. Zhou, B. Song, C. Lu, X. Yan, X. Li, F. Huang, S. Yin, P. J. Stang, *J. Am. Chem. Soc.***2017**, *139*, 5067-5074; d) A. Casini, B. Woods, M. Wenzel, *Inorg. Chem.* **2017**, *56*, 14715-14729; e) Q.-Q. Wang, S. Gonell, S. H. A. M. Leenders, M. Dürr, I. Ivanović-Burmazović, J. N. H. Reek, *Nat. Chem.* **2016**, *8*, 225-230; f) C. J. Brown, F. D. Toste, R. G. Bergman, K. N. Raymond, *Chem. Rev.* **2015**, *115*, 3012-3035; g) J. Wang, C. He, P. Wu, J. Wang, C. Duan, *J. Am. Chem. Soc.***2011**, *133*, 12402-12405; h) P. Mal, B. Breiner, K. Rissanen, J. R. Nitschke, *Science* **2009**, *324*, 1697-1699.

[6] a) K. A. Dill, J. L. MacCallum, *Science* **2012**, *338*, 1042-1046; b) F. U. Hartl, A. Bracher, M. Hayer-Hartl, *Nature* **2011**, *475*, 324-332.

[7] S. R. Seidel, P. J. Stang, *Acc. Chem. Res.* **2002**, *35*, 972-983.

[8] M. Yoshizawa, L. Catti, *Acc. Chem. Res.* **2019**, *52*, 2392-2404.

[9] J. E. M. Lewis, J. D. Crowley, *ChemPlusChem* **2020**, *85*, 815-827.

[10] a) J. Tessarolo, H. Lee, E. Sakuda, K. Umakoshi, G. H. Clever, *J. Am. Chem. Soc.***2021**, *143*, 6339-6344; b) S. Sudan, R.-J. Li, S. M. Jansze, A. Platzek, R. Rudolf, G. H. Clever, F. Fadaei-Tirani, R. Scopelliti, K. Severin, *J. Am. Chem. Soc.* **2021**, *143*, 1773-1778; c) S. Pullen, J. Tessarolo, G. H. Clever, *Chem. Sci.* **2021**, *12*, 7269-7293; d) S. Saha, B. Holzapfel, Y.-T. Chen, K. Terlinden, P. Lill, C. Gatsogiannis, H. Rehage, G. H. Clever, *J. Am. Chem. Soc.* **2018**, *140*, 17384-17388; e) S. Pullen, G. H. Clever, *Acc. Chem. Res.* **2018**, *51*, 3052-3064; f) W. M. Bloch, Y. Abe, J. J. Holstein, C. M. Wandtke, B. Dittrich, G. H. Clever, *J. Am. Chem. Soc.* **2016**, *138*, 13750-13755; g) Y. K. Kryschenko, S. R. Seidel, D. C. Muddiman, A. I. Nepomuceno, P. J. Stang, *J. Am. Chem. Soc.* **2003**, *125*, 9647-9652.

[11] a) J. E. M. Lewis, *Chem. Eur. J.* **2021**, *27*, 4454-4460; b) S. S. Mishra, S. V. K. Kompella, S. Krishnaswamy, S. Balasubramanian, D. K. Chand, *Inorg. Chem.* **2020**, *59*, 12884-12894; c) L. S. Lisboa, J. A. Findlay, L. J. Wright, C. G. Hartinger, J. D. Crowley, *Angew. Chem. Int. Ed.* **2020**, *59*, 11101-11107; d) J. E. M. Lewis, A. Tarzia, A. J. P. White, K. E. Jelfs, *Chem. Sci.* **2020**, *11*, 677-683; e) B. Chen, S. Horiuchi, J. J. Holstein, J. Tessarolo, G. H. Clever, *Chem. Eur. J.* **2019**, *25*, 14921-14927; f) D. Preston, J. E. Barnsley, K. C. Gordon, J. D. Crowley, *J. Am. Chem. Soc.* **2016**, *138*, 10578-10585. g) S. Löffler, J. Lübben, A. Wuttke, R. A. Mata, M. John, B. Dittrich, G. H. Clever, *Chem. Sci.* **2016**, *7*, 4676-4684. h) S. E. Walker, S. A. Boer, T. Malcomson, M. J. Paterson, K. L. Tuck, D. R. Turner, *Chem. Commun*. **2021**, 57, 12456-12459.

[12] C.-L. Liu, E. O. Bobylev, Y. Fu, D. A. Poole Iii, K. Robeyns, C.-A. Fustin, Y. Garcia, J. N. H. Reek, M. L. Singleton, *Chem. Eur. J.* **2020**, *26*, 11960-11965.

[13] a) F. Kerff, C.-L. Liu, X. Mu, U. Gilbert, L. Smal, L. Meinertzhagen, B. Kauffmann, K. Robeyns, M. L. Singleton, *ChemPlusChem* **2021**, *86*, 1162-1166; b) E. Berni, B. Kauffmann, C. Bao, J. Lefeuvre, D. M. Bassani, I. Huc, *Chem. Eur. J.* **2007**, 13, 8463-8469.

[14] a) S. M. Jansze, G. Cecot, M. D. Wise, K. O. Zhurov, T. K. Ronson, A. M. Castilla, A. Finelli, P. Pattison, E. Solari, R. Scopelliti, G. E. Zelinskii, A. V. Vologzhanina, Y. Z. Voloshin, J. R. Nitschke, K. Severin, *J. Am. Chem. Soc.* **2016**, *138*, 2046-2054; b) A. M. Johnson, C. A. Wiley, M. C. Young, X. Zhang, Y. Lyon, R. R. Julian, R. J. Hooley, *Angew. Chem. Int. Ed.* **2015**, *54*, 5641-5645; c) Q.-F. Sun, J. Iwasa, D. Ogawa, Y. Ishido, S. Sato, T. Ozeki, Y. Sei, K. Yamaguchi, M. Fujita, *Science* **2010**, *328*, 1144-1147.

[15] M. Morimoto, S. M. Bierschenk, K. T. Xia, R. G. Bergman, K. N. Raymond, F. D. Toste, *Nat. Catal.* **2020**, *3*, 969-984.

[16] M. L. Singleton, N. Castellucci, S. Massip, B. Kauffmann, Y. Ferrand, I. Huc, *J. Org. Chem.* **2014**, *79*, 2115-2122.

[17] a) Y. Fang, J. A. Powell, E. Li, Q. Wang, Z. Perry, A. Kirchon, X. Yang, Z. Xiao, C. Zhu, L. Zhang, F. Huang, H.-C. Zhou, *Chem. Soc. Rev.* **2019**, *48*, 4707-4730; b) J. Lee, O. K. Farha, J. Roberts, K. A. Scheidt, S. T. Nguyen, J. T. Hupp, *Chem. Soc. Rev.* **2009**, *38*, 1450-1459.

[18] E. O. Bobylev, D. A. Poole Iii, B. de Bruin, J. N. H. Reek, *Chem. Sci.* **2021**, *12*, 7696-7705.

[19] a) L. He, H. Li, J. Chen, X.-F. Wu, *RSC Adv.* **2014**, *4*, 12065-12077; b) Z. Xu, Y. Zhang, H. Fu, H. Zhong, K. Hong, W. Zhu, *Bioorg. Med. Chem. Lett.* **2011**, *21*, 4005-4007; c) G. M. Chinigo, M. Paige, S. Grindrod, E. Hamel, S. Dakshanamurthy, M. Chruszcz, W. Minor, M. L. Brown, *J. Med. Chem.* **2008**, *51*, 4620-4631.

[20] a) C. Tan, K. Yang, J. Dong, Y. Liu, Y. Liu, J. Jiang, Y. Cui, *J. Am. Chem. Soc.* **2019**, *141*, 17685-17695; b) G. K. Kharmawlong, R. Nongrum, B. Chhetri, J. W. S. Rani, N. Rahman, A. K. Yadav, R. Nongkhlaw, *Synth. Commun.* **2019**, *49*, 2683-2695; c) J. Jiao, Z. Li, Z. Qiao, X. Li, Y. Liu, J. Dong, J. Jiang, Y. Cui, *Nat. Commun.* **2018**, *9*, 4423; d) M. Rueping, A. P. Antonchick, E. Sugiono, K. Grenader, *Angew. Chem. Int. Ed.* **2009**, *48*, 908-910.

[21] a) C. Ngai, C. M. Sanchez-Marsetti, W. H. Harman, R. J. Hooley, *Angew. Chem. Int. Ed.* **2020**, *59*, 23505-23509; b) J. Yang, B. Chatelet, V. Dufaud, D. Hérault, S. Michaud-Chevallier, V. Robert, J.-P. Dutasta, A. Martinez, *Angew. Chem. Int. Ed.* **2018**, *57*, 14212-14215; c) L. R. Holloway, P. M. Bogie, Y. Lyon, C. Ngai, T. F. Miller, R. R. Julian, R. J. Hooley, *J. Am. Chem. Soc.* **2018**, *140*, 8078-8081; d) T. Akiyama, K. Mori, *Chem. Rev.* **2015**, *115*, 9277-9306; e) S. R. Shenoy, F. R. Pinacho Crisóstomo, T. Iwasawa, J. Rebek, *J. Am. Chem. Soc.* **2008**, *130*, 5658-5659.

Entry for the Table of Contents

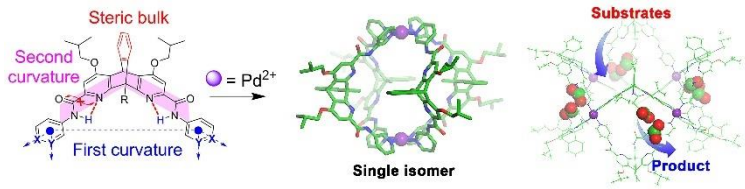

A combination of aromatic amide ligands containing endohedral non-covalent interactions and increased shape complementarity brought by the addition of a second curvature to the ligand structure provides an effective strategy for controlling palladium based self-assembly with flexible and low symmetry non-planar ligands.